Graduate University of Advanced Technology

Journal of Geological Remote Sensing

Journal homepage: https:// jgrs.kgut.ac.ir

Iranian Geological Remote Sensing Society

Investigation of the Support Vector Machine (SVM) algorithm for land use changes, a case study of Kerman Province, Iran

Mahdi Dehghananari[1], Mahdieh Hosseinjanizadeh[2*]

[1] *Bachelor's student, Civil Engineering Department, Shahid Bahonar University of Kerman, Kerman, Iran*
[2] *Associate Professor, Department of Ecology, Institute of Science and High Technology and Environmental Sciences, Graduate University of Advanced Technology, Kerman, Iran*

Article Info

Keywords:
Remote Sensing
Landsat satellite imagery
Land use and land cover
Climate change
Human activities

Abstract

Land use and land cover (LULC) play a crucial role in studying the ongoing worldwide environmental changes This study employs TM, ETM+, and OLI images acquired from the Landsat satellite over a thirty-year period (1990-2020) to analyze changes in land use. The Support Vector Machine (SVM) algorithm is utilized for land use classification, and a Median filter in the ENVI software was applied to the SVM algorithm results to produce smoother images. The study area is located in Kerman Province, Iran, encompassing the cities of Kerman, Zarand, Bardsir, and parts of Rafsanjan, Ravar, and Sirjan counties. Four classes were selected for SVM classification: built-up areas, vegetation, water resources, and bare land (comprising soil and rock formations). The results indicated that the classification of OLI data performs better in terms of overall accuracy (more than 80%) and the kappa coefficient (more than 0.7). Specifically, the analysis revealed a 1.88% decrease in vegetation cover, a 0.19% increase in urban areas, and a 0.005% change in surface water bodies over the 30-year period. These changes are attributed to the influence of human activities, drought, poor management practices, and climate change on the dynamics of land use in the region.

*Corresponding author: Mahdieh Hosseinjanizadeh
Email: *mh.hosseinjani@gmail.com*

https://doi.org/10.48306/jgrs.2024.467600.1009
Received July. 2024; Received in revised form September. 2024; Accepted: October 2024
Available online November 2024

1. Introduction

The Industrial Revolution marked the beginning of a new epoch, the Anthropocene,(1), characterized by human activity as the primary driver of global environmental changes (2). Land use and land cover (LULC) are fundamental parameters in the study of the ongoing global environmental changes (3). LULC refers to the utilization of land for agriculture, wildlife habitats, urban areas, and any other activities resulting from the interaction between humans and the environment in a specific locale (4, 5) (6). The 20th century saw significant urban development, driven by human activities, which profoundly altered the LULC change process (7, 8). As a result, understanding changes in land use patterns and their drivers has become a critical challenge in LULC science (9, 10). Consequently, assessing LULC changes is essential for human well-being, particularly in the face of rapid and uncontrolled population growth. Especially in developing countries where LULC changes are more intense (11, 12) (13, 14). Remote sensing can produce useful spectral reflectance data that provides a quick tool for managing and monitoring natural resources and determination of land use and land cover changes (15).

Landsat images are one of the longest and most widely used datasets for geospatial data analysis. These images have an average spatial resolution of about 30 meters per pixel of the earth's surface (16). Since the launch of the first Landsat satellite in 1972 (17), a variety of classification algorithms have been developed in remote sensing for the classification of Earth's activities (18-21). The reason for the popularity of NASA's Landsat mission data is its free access and long-term global coverage. So, these data are among the effective solutions in terms of cost and time (22-25).

In general, the logical classifications of satellite images are based on parametric and non-parametric categories which both algorithms are mainly pixel-oriented in the science of remote sensing (26). In parametric classification, the data for individual classes are assumed to be normally distributed and employ a fixed-form decision boundary (27). This implies that the distribution is more concentrated around the mean, such as maximum likelihood classification as the most popular in this category (28). However, when the region delineated by the classified training sample exhibits complex boundaries, such classification is likely to result in a noisy output, where the classified pixels are incorrectly separated (29). The other category includes non-parametric classification that does not make any assumptions about the statistical nature of the data (30). This feature is suitable for areas with different classes where the available data are often not normally distributed (31). The classification algorithm of satellite imagery can be divided also into two categories including; supervised and unsupervised classification. In supervised classification, the identity and location of some areas under investigation are known, for example, agricultural, urban, etc. Conversely, in unsupervised classification, the absence of prior knowledge about the area leads the computer to group pixels with similar spectral properties into clusters (32).

Support Vector Machine (SVM) is a non-parametric and supervised classifier system that has attracted the attention of researchers in the last two decades (33, 34) (35). SVM, which was first proposed by Vapnik and Chervonenkis (1971), gained popularity due to its strong theoretical foundations (36). This algorithm implements the idea that transforms the input data x into the high-dimensional feature space through non-linear mappings (37). SVM is a result of statistical learning theory and differentiates the classes with the decision surface known as the optimal hyperline. This hyperline makes the difference between the classes more visible (38). The purpose of SVM is to generate a model based on the training data that predicts the target values only according to the characteristics of the test data (38). In addition, SVM is an abstraction of a machine learning algorithm that utilizes a series of datasets to attempt to generalize across other datasets and make accurate predictions (39, 40). In many scientific applications, SVM has a higher accuracy of long-term prediction compared to other computational methods (41). The SVM algorithm has been used in numerous studies for different applications including; in the field of land subsidence (42), Prediction of flow discharge (43), Medical science (44-46), hydrothermal alternation mapping (47, 48), estimating the diffuse solar radiation (49, 50), mining (51-56) and especially Land Use Land Cover maps (57-61). Despite the development of SVM, few studies have been used for the preparation of LULC maps through this algorithm, especially in the study area. The purpose of the current study is to investigate the Support Vector Machine (SVM) algorithm for land use classification within 30 years (1990-2020) through Landsat images in the Kerman region. The escalating impacts of climate change and drought require more extraordinary measures for resource management to ensure human well-being, particularly in arid and desert regions. The Kerman region, located in such an environment, is particularly vulnerable and requires further investigation to address these challenges effectively. The changes in urban areas, rangelands, agricultural vegetation, and water resources as well as the impact of Human activities were determined. The results provide a strong basis for upcoming work and could help to manage land and protect the environment in areas undergoing rapid changes.

2. Study area

The studied area is a part of Kerman province located in the southeast sector of Iran. This region includes the counties of Kerman, Zarand, Rafsanjan, Bardsir, and parts of Sirjan and Ravar; with an average elevation of about 1633 meters above the sea level. The study area covers between latitude 29˚ 32' to 30˚ 59' N and longitude 56˚ 08' to 57˚ 21' E with an area of about 18360 Km^2 *(Figure 1).* According to the extended De Martonne classification system, the counties of Kerman, Zarand, and Sirjan have arid cold climate, and the counties of Rafsanjan, Raver, and Bardsir respectively have arid moderate, arid warm, and semi-arid cold climate (62). In general, Kerman province has a cold desert climate with hot summers and cool to cold winters with low amount of rainfall throughout the year (63). According to the last census conducted in 2016, the population of this province is estimated at 3164718. The most prevalent land uses in this area are residential, agricultural, and industrial.

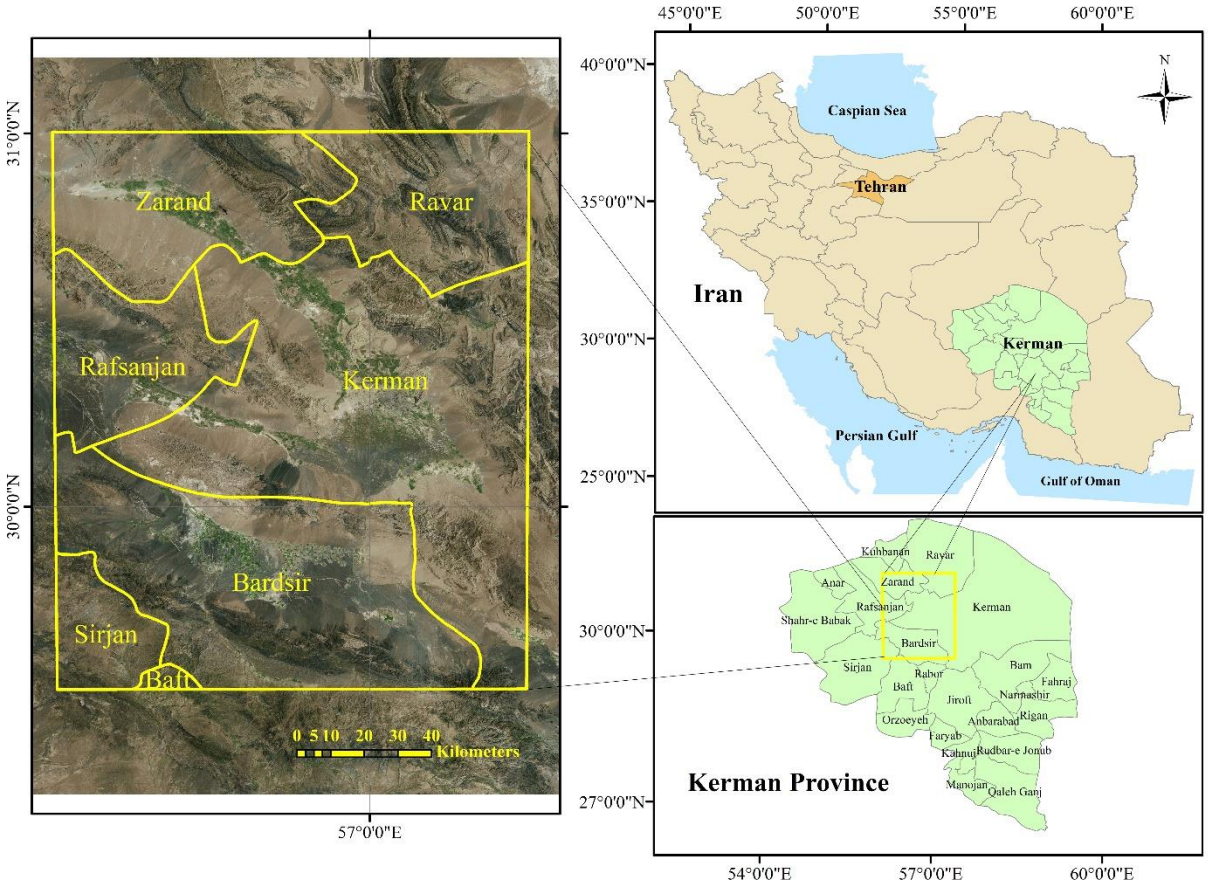

Figure 1. Location of the study area.

3. Material and methods

Landsat 5 (TM), 7 (ETM+), and, 8 (OLI) images were acquired from the United States Geological Survey (USGS) website for a period of thirty years (1990-2020) in this study. Landsat images spanning 5-year intervals have been utilized to simplify the comparison process (Table 1). Furthermore, the maximum cloud coverage in the selected images is 1%. The images were chosen from the early summer months of June and July, when there is a lower likelihood of cloud presence and a higher probability of dense vegetation cover, to enhance the accuracy of image processing.

Table 1. The information of the images used in this study.

S. No	Year / month	Satellite / Sensor Product
1	1990/06/17	Landsat 5 / TM
2	1995/06/15	Landsat 5 / TM
3	2000/07/22	Landsat 7 / ETM+
4	2005/06/02	Landsat 7 / ETM+
5	2010/07/02	Landsat 7 / ETM+
6	2015/06/06	Landsat 8 / OLI
7	2020/07/21	Landsat 8 / OLI

The data analysis procedure includes the following steps: a) Image Acquisition, b) Radiometric Calibration, c) Atmospheric Calibration, d) Cropping images for the study area, e) Applying the SVM Algorithm, f) Applying a filter, and g) Accuracy Assessment (Figure 2). Radiometric calibration is used to convert the digital number (DN) of satellite images into spectral radiance and reflectance (64). This correction is crucial for the quantification of remote sensing data (65). The atmospheric correction, which is needed to remove the effects of atmospheric absorption and scattering (66), was performed using the Fast Line-of-Sight Atmospheric Analysis of Spectral Hypercubes (FLAASH) algorithm. FLAASH algorithm is a tool for atmospheric correction that gives the user limited control in setting the input parameters. This tool is easy to use by setting appropriate input parameters that specify atmospheric conditions and illumination/viewing geometry at the time of image capture (67). It is important to note that for Landsat 7 satellite images captured from 2003 onwards, a Gap-filled product was utilized due to the scan line corrector being off. Gap-filled products compile data from multiple ETM^+ scenes to ensure complete terrain coverage (68). Subsequently, the images are cropped according to the research area, and the SVM algorithm is applied to generate a classification map. Four major classes were determined including; 1) Vegetation, 2) Bare land (including soil and rock formations), 3) Urban areas (including cities and buildings), and 4) Water. These classes represent the most significant and distinct types of land cover that are crucial for various analyses.

The SVM algorithm, as a default algorithm in ENVI software, uses non-linear Kernel functions for classification. Kernels are used to map data into new space (69). The type of kernel used in this research is the Radial Basis Function (RBF), which has performed well in most cases(70).

$K(x_i,x_j)=exp(-\gamma\|x_i- x_j \|^2), \gamma >0$

Where:

K (xi, xj) is the kernel function evaluating the similarity between two data points xi and xj.

xi and xj are the input data points.

γ (gamma) is a hyperparameter that controls the width of the kernel.

‖xi - xj‖ is the Euclidean distance between xi and xj.

exp is the exponential function.

The output results of the SVM algorithm contain noises that have been reduced by applying a filter. The filter applied to the resulting classified images is a type of convolution filter available in ENVI software. This convolution filter produces outputs where the brightness value of a given pixel is a function of the weighted average of brightness values from surrounding pixels. In this research, a median filter from ENVI software was employed, which replaces the central pixel with the median value (not the average) within the neighborhood defined by the filter size. The kernel size utilized for this filter was 7x7 and this filter yields a smoother image with reduced noise (70). Ultimately, the accuracy of the training data was assessed using reference data, including satellite images from the Google mapping

service, Google Earth, and by calculating the Kappa coefficient and overall accuracy. It should be noted that these data were taken separately for each year.

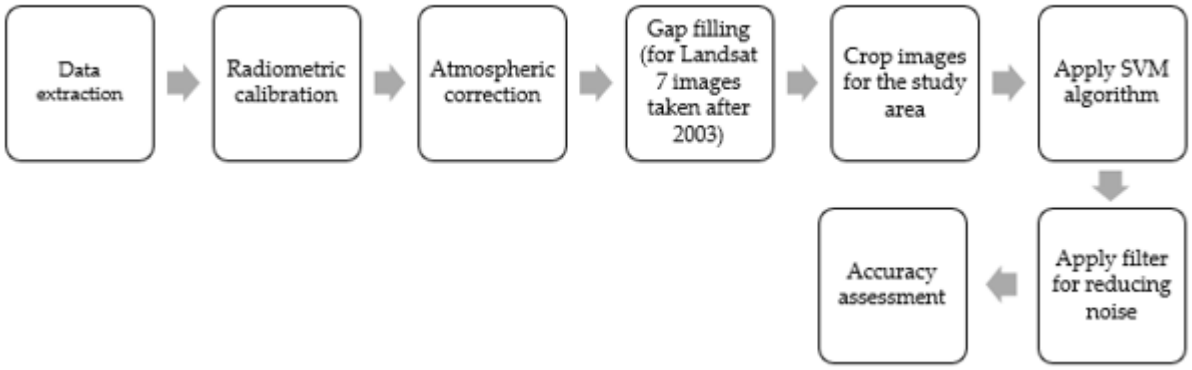

Figure 2. Flowchart of methodology.

4. Results and Discussion

Landsat series satellite images were utilized to produce a classified map using the SVM algorithm in this research. The results clearly indicate that vegetation has experienced changes over the 30-year period (Figure 3). The trend has been predominantly downward since 1990 (Figure 3 g), as shown by the decrease in vegetation cover from approximately 5.58% in 1990 to 3.7% by 2020 (Figure 3 a) (Table 2)

The majority of the area consists of bare land, comprising soil and rock formations, which increased from 94% in 1990 to nearly 96% in 2020. The data derived from the classified map suggest that urban areas expanded from 0.19% in 1990 to 0.38% in 2020. However, irregular trends were observed before 2010, particularly in 1995, where misclassification occurred in the urban and bare land categories. The misclassification data were checked several times and the algorithm was run by changing the classes, and visible errors still appeared in the output. Consequently, some regions initially classified as urban were actually part of the bare land category. This misclassification can be attributed to the relative similarity in the reflected radiation from urban and bare land areas in this region. The findings also show that there was almost no surface water in the study area until 2000, and after that, a very small amount of water was distinguished from 2005 to 2020. The delineated water, when exported to Google Earth, corresponded to the locations of dams constructed at the Chahar Gonbad and Takht Gonbad copper mines in the southern part of the study area, which were built after 2000 and 2010, respectively (Figure 3, a-e).

Table 2. Percentage of LULC map classification classes over thirty years

Year	Vegetation %	Water %	Bare land %	Urban %
2020	3.7	0.005	95.92	0.38
2015	4.96	0.003	94.73	0.31
2010	5.41	0.01	94.21	0.37
2005	5.58	0.02	94.24	0.16
2000	5.7	0	93.93	0.38
1995	5.34	0	93.43	1.23
1990	5.58	0	94.23	0.19

The results presented in Table 2 suggest that the rate of vegetation decline has intensified, which may be attributed to population growth, poor management practices, and even climate change. Inadequate management of human activities, such as urban development, construction, and dam building, has significantly impacted the ecosystem and vegetation of the region. Additionally, the over-extraction of groundwater through well drilling is a contributing factor to vegetation loss. Moreover, climate change, regarded as one of the gravest environmental challenges globally (71, 72), can lead to increased temperatures and consequently the desiccation of surface water resources, vegetation, and soil (73). A particular manifestation of climate change in Iran is the escalating severity of droughts, coupled with a decrease in rainfall and the magnitude of floods (74). The area under study has endured severe drought over the past two decades (75). According to the report from the General Department of Meteorology of Kerman Province, climate change has influenced the temperature and precipitation levels in the region. The report indicates that the average temperature approximately rose from 19°C in 1990 to 20°C in 2020, with an upward trend of 0.5°C per decade. Furthermore, the report notes a decrease in rainfall, with a downward trend of roughly 13 mm per decade over the same 30-year span (76). An investigation of the kappa coefficient and overall accuracy demonstrated a strong concordance between the classified map and the reference data (Table 3). The results indicate that the kappa coefficient and overall accuracy for Landsat TM data are lower compared to those for ETM^{+} and OLI, with the most reliable results obtained from OLI Landsat 8.

Table 3. Kappa coefficient and overall accuracy percentage of LULC images.

Year	Kappa Coefficient	Overall Accuracy %
2020	0.75	83.67
2015	0.70	80.52
2010	0.84	80.69
2005	0.63	76.22
2000	0.62	76.51
1995	0.56	72.29
1990	0.51	69

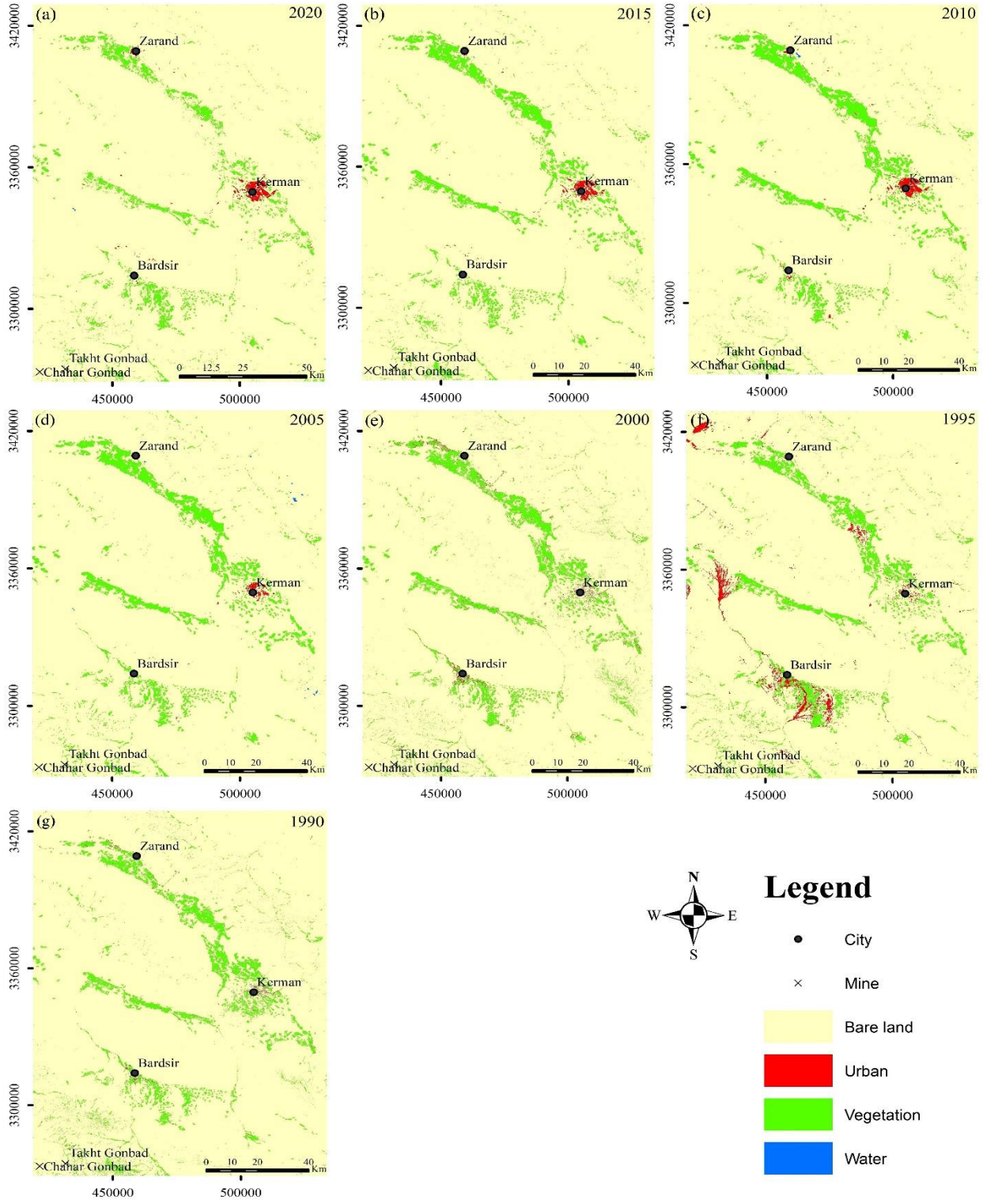

Figure 3. Land classification maps of the study area in the 30-year period by SVM algorithm. (a) Discrement area of 2020, Landsat 8 OLI sensor. (b) Discrement area of 2015, Landsat 8 OLI sensor. (c) Discrement area of 2010, Landsat 7 ETM+ sensor.(d) Discrement area of 2005, Landsat 7 ETM+ sensor. (e) Discrement area of 2000, Landsat 7 ETM+ sensor. (f) Discrement area of 1995, Landsat 5 TM sensor. (g) Discrement area of 1990, Landsat 5 TM sensor.

5. Conclusion

In this paper, land use changes are analyzed using Landsat satellite imagery over three decades, employing the SVM algorithm in conjunction with a Median filter in ENVI software. The classification was conducted across four categories: built-up areas, plant life, water bodies, and bare land. The results reveal that the algorithm initially struggled to differentiate between built-up areas and bare land, especially for TM data; however, this issue was significantly resolved in classified images obtained from Landsat ETM^+ and OLI data. Furthermore, the findings demonstrate a decrease in vegetation and an expansion of urban areas, shedding light on the significant impact of human activities, climate change, drought, and environmental management practices. The study underscores the efficacy of the SVM algorithm in land use classification and its potential for precise and reliable remote sensing applications. The acceptable level of accuracy attained with the SVM algorithm, especially with Landsat 8 OLI data, affirms its appropriateness for monitoring and managing land use dynamics. These insights have important implications for environmental research and demonstrate the potential of SVM-based methods for monitoring and mitigating the effects of land use changes.

6. References

1. Crutzen PJ. Geology of mankind. Paul J Crutzen: A pioneer on atmospheric chemistry and climate change in the Anthropocene. 2016:211-5.
2. Steffen W, Crutzen PJ, McNeill JR. The Anthropocene: are humans now overwhelming the great forces of nature. Ambio-Journal of Human Environment Research and Management. 2007;36(8):614-21.
3. Manandhar R, Odeh IO, Pontius Jr RG. Analysis of twenty years of categorical land transitions in the Lower Hunter of New South Wales, Australia. Agriculture, ecosystems & environment. 2010;135(4):336-46.
4. Rawat J, Kumar M. Monitoring land use/cover change using remote sensing and GIS techniques: A case study of Hawalbagh block, district Almora, Uttarakhand, India. The Egyptian Journal of Remote Sensing and Space Science. 2015;18(1):77-84.
5. Prakasam C. Land use and land cover change detection through remote sensing approach: A case study of Kodaikanal taluk, Tamil nadu. International journal of Geomatics and Geosciences. 2010;1(2):150.
6. Reis S. Analyzing land use/land cover changes using remote sensing and GIS in Rize, North-East Turkey. Sensors. 2008;8(10):6188-202.
7. Aboelnour M, Engel BA. Application of remote sensing techniques and geographic information systems to analyze land surface temperature in response to land use/land cover change in Greater Cairo Region, Egypt. Journal of Geographic Information System. 2018;10(1):57-88.

8. Sajib AM, Moniruzzaman M. Driving forces of landuse and landcover changes in the north-eastern part of Dhaka Conurbation. The Dhaka University Journal of Earth and Environmental Sciences. 2021;10(2):53-66.
9. Moran EF, Ojima D, McConnell W, Stafford Smith M, Laumann G, Morais J, Young B. Global land project: Science plan and implementation strategy. IGBP report. 2005;53.
10. Turner BL, Lambin EF, Reenberg A. The emergence of land change science for global environmental change and sustainability. Proceedings of the National Academy of Sciences. 2007;104(52):20666-71.
11. Dutta D, Rahman A, Paul S, Kundu A. Changing pattern of urban landscape and its effect on land surface temperature in and around Delhi. Environmental monitoring and assessment. 2019;191:1-15.
12. Thanh Hoan N, Liou Y-A, Nguyen K-A, Sharma RC, Tran D-P, Liou C-L, Cham DD. Assessing the effects of land-use types in surface urban heat islands for developing comfortable living in Hanoi City. Remote Sensing. 2018;10(12):1965.
13. Rahman A, Aggarwal SP, Netzband M, Fazal S. Monitoring urban sprawl using remote sensing and GIS techniques of a fast growing urban centre, India. IEEE Journal of selected topics in applied earth observations and remote sensing. 2010;4(1):56-64.
14. Shahfahad, Kumari B, Tayyab M, Hang HT, Khan MF, Rahman A. Assessment of public open spaces (POS) and landscape quality based on per capita POS index in Delhi, India. SN Applied Sciences. 2019;1:1-13.
15. Da Silva VS, Salami G, da Silva MIO, Silva EA, Monteiro Junior JJ, Alba E. Methodological evaluation of vegetation indexes in land use and land cover (LULC) classification. Geology, Ecology, and Landscapes. 2020;4(2):159-69.
16. Lane GJ, Goresen P, Slater R. Repairing Landsat satellite imagery using deep machine learning techniques. SMU Data Science Review. 2019;2(1):12.
17. Wulder MA, White JC, Loveland TR, Woodcock CE, Belward AS, Cohen WB, et al. The global Landsat archive: Status, consolidation, and direction. Remote Sensing of Environment. 2016;185:271-83.
18. Townshend JG. Land cover. International Journal of Remote Sensing. 1992;13(6-7):1319-28.
19. Rai AK, Mandal N, Singh A, Singh KK. Landsat 8 OLI satellite image classification using convolutional neural network. Procedia Computer Science. 2020;167:987-93.
20. Maxwell AE, Warner TA, Fang F. Implementation of machine-learning classification in remote sensing: An applied review. International journal of remote sensing. 2018;39(9):2784-817.
21. Bruzzone L, Demir B. A review of modern approaches to classification of remote sensing data. Land Use and Land Cover Mapping in Europe: Practices & Trends. 2014:127-43.
22. Barnsley MJ, Barr SL. Inferring urban land use from satellite sensor images using kernel-based spatial reclassification. Photogrammetric engineering and remote sensing. 1996;62(8):949-58.

23. Erener A, Düzgün S, Yalciner AC. Evaluating land use/cover change with temporal satellite data and information systems. Procedia Technology. 2012;1:385-9.
24. Güler M, Yomralıoğlu T, Reis S. Using landsat data to determine land use/land cover changes in Samsun, Turkey. Environmental monitoring and assessment. 2007;127:155-67.
25. Yang X, Liu Z. Use of satellite-derived landscape imperviousness index to characterize urban spatial growth. Computers, Environment and Urban Systems. 2005;29(5):524-40.
26. Wieland M, Pittore M. Performance evaluation of machine learning algorithms for urban pattern recognition from multi-spectral satellite images. Remote Sensing. 2014;6(4):2912-39.
27. Srivastava PK, Han D, Rico-Ramirez MA, Bray M, Islam T. Selection of classification techniques for land use/land cover change investigation. Advances in Space Research. 2012;50(9):1250-65.
28. Richards JA, Richards JA. Remote sensing digital image analysis: Springer; 2022.
29. Hubert-Moy L, Cotonnec A, Le Du L, Chardin A, Pérez P. A comparison of parametric classification procedures of remotely sensed data applied on different landscape units. Remote Sensing of Environment. 2001;75(2):174-87.
30. LeMay V, Temesgen H. Comparison of nearest neighbor methods for estimating basal area and stems per hectare using aerial auxiliary variables. Forest Science. 2005;51(2):109-19.
31. Abedi R. Comparison of parametric and non-parametric techniques to accurate classification of forest attributes on satellite image data. Journal of Environmental Science Studies. 2020;5(4):3229-35.
32. Jensen JR. Introductory digital image processing: a remote sensing perspective. 1996.
33. Chen S-T. Mining informative hydrologic data by using support vector machines and elucidating mined data according to information entropy. Entropy. 2015;17(3):1023-41.
34. Vapnik V. Estimation of dependences based on empirical data: Springer Science & Business Media; 2006.
35. Mountrakis G, Im J, Ogole C. Support vector machines in remote sensing: A review. ISPRS Journal of Photogrammetry and Remote Sensing. 2011;66(3):247-59.
36. Niroomand MP, Morgan JW, Cafolla CT, Wales DJ. On the capacity and superposition of minima in neural network loss function landscapes. Machine Learning: Science and Technology. 2022;3(2):025004.
37. Vapnik VN, Vapnik V. Statistical learning theory. 1998.
38. Hsu C-W, Chang C-C, Lin C-J. A practical guide to support vector classification. Taipei; 2003.
39. Campbell C, Ying Y. Learning with support vector machines: Springer Nature; 2022.
40. Settles B. Active learning (synthesis lectures on artificial intelligence and machine learning)(morgan and claypool publishers, san rafael, ca). 2012.
41. Deris AM, Zain AM, Sallehuddin R. Overview of support vector machine in modeling machining performances. Procedia Engineering. 2011;24:308-12.

42. Abdollahi S, Pourghasemi HR, Ghanbarian GA, Safaeian R. Prioritization of effective factors in the occurrence of land subsidence and its susceptibility mapping using an SVM model and their different kernel functions. Bulletin of Engineering Geology and the Environment. 2019;78:4017-34.
43. Samantaray S, Sahoo A. Prediction of flow discharge in Mahanadi River Basin, India, based on novel hybrid SVM approaches. Environment, Development and Sustainability. 2024;26(7):18699-723.
44. Ali L, Javeed A, Noor A, Rauf HT, Kadry S, Gandomi AH. Parkinson's disease detection based on features refinement through L1 regularized SVM and deep neural network. Scientific Reports. 2024;14(1):1333.
45. Altin FG, Budak İ, Özcan F. Predicting the amount of medical waste using kernel-based SVM and deep learning methods for a private hospital in Turkey. Sustainable Chemistry and Pharmacy. 2023;33:101060.
46. Modhugu VR, Ponnusamy S. Comparative Analysis of Machine Learning Algorithms for Liver Disease Prediction: SVM, Logistic Regression, and Decision Tree. Asian Journal of Research in Computer Science. 2024;17(6):188-201.
47. Mojeddifar S, Mavadati M. Integration of support vector machines for hydrothermal alteration mapping using ASTER data–case study: the northwestern part of the Kerman Cenozoic Magmatic Arc, Iran. International Journal of Mining and Geo-Engineering. 2020;54(1):45-50.
48. Xu K, Wang X, Kong C, Feng R, Liu G, Wu C. Identification of hydrothermal alteration minerals for exploring gold deposits based on SVM and PCA using ASTER data: A case study of Gulong. Remote Sensing. 2019;11(24):3003.
49. Fan J, Wu L, Zhang F, Cai H, Wang X, Lu X, Xiang Y. Evaluating the effect of air pollution on global and diffuse solar radiation prediction using support vector machine modeling based on sunshine duration and air temperature. Renewable and Sustainable Energy Reviews. 2018;94:732-47.
50. Shamshirband S, Mohammadi K, Khorasanizadeh H, Yee L, Lee M, Petković D, Zalnezhad E. Estimating the diffuse solar radiation using a coupled support vector machine–wavelet transform model. Renewable and Sustainable Energy Reviews. 2016;56:428-35.
51. He D, Le BT, Xiao D, Mao Y, Shan F, Ha TTL. Coal mine area monitoring method by machine learning and multispectral remote sensing images. Infrared Physics & Technology. 2019;103:103070.
52. Liu W, Ren Y, Meng X, Tian B, Lv X. Analysis of potential water inflow rates at an underground coal mine using a WOA-CNN-SVM approach. Water. 2024;16(6):813.
53. Luo X, Lin F, Zhu S, Yu M, Zhang Z, Meng L, Peng J. Mine landslide susceptibility assessment using IVM, ANN and SVM models considering the contribution of affecting factors. PloS one. 2019;14(4):e0215134.
54. Mohammadzadeh M, Mohebbi P. An orientation survey for methodizing classification accuracy of Cu mineralization by hybrid methods of fractal, neural networks, and support vector machine in Haftcheshmeh, NW Iran. Arabian Journal of Geosciences. 2018;11(20):618.

55. Mukherjee J, Mukherjee J, Chakravarty D, Aikat S. A novel index to detect opencast coal mine areas from Landsat 8 OLI/TIRS. IEEE Journal of Selected Topics in Applied Earth Observations and Remote Sensing. 2019;12(3):891-7.
56. Raval S, Shamsoddini A. A monitoring framework for land use around kaolin mining areas through Landsat TM images. Earth Science Informatics. 2014;7:153-63.
57. Al-doski J, Mansor SB, Shafri HZ, editors. Support vector machine classification to detect land cover changes in Halabja City, Iraq. 2013 IEEE Business Engineering and Industrial Applications Colloquium (BEIAC); 2013: IEEE.
58. Halder S, Das S, Basu S. Use of support vector machine and cellular automata methods to evaluate impact of irrigation project on LULC. Environmental Monitoring and Assessment. 2023;195(1):3.
59. Jamali A. Land use land cover modeling using optimized machine learning classifiers: a case study of Shiraz, Iran. Modeling Earth Systems and Environment. 2021;7(3):1539-50.
60. Karimi F, Sultana S, Babakan AS, Suthaharan S. An enhanced support vector machine model for urban expansion prediction. Computers, Environment and Urban Systems. 2019;75:61-75.
61. Rana VK, Suryanarayana TMV. Performance evaluation of MLE, RF and SVM classification algorithms for watershed scale land use/land cover mapping using sentinel 2 bands. Remote Sensing Applications: Society and Environment. 2020;19:100351.
62. Bakhtiari B, Bakhtiari A. Determination of tourism climate index in Kerman province. 2013.
63. Beck HE, Zimmermann NE, McVicar TR, Vergopolan N, Berg A, Wood EF. Present and future Köppen-Geiger climate classification maps at 1-km resolution. Scientific data. 2018;5(1):1-12.
64. Suyarso S, Setiawati MD, Supriyadi IH, Prayudha B. Climate change indicator, impact, adaptation, and innovation at the local level: learn from the peoples' experience of the coastal plain of Probolinggo, East Java, Indonesia. Climate Change, Community Response and Resilience: Elsevier; 2023. p. 93-118.
65. Deng L, Hao X, Mao Z, Yan Y, Sun J, Zhang A. A subband radiometric calibration method for UAV-based multispectral remote sensing. IEEE Journal of Selected Topics in Applied Earth Observations and Remote Sensing. 2018;11(8):2869-80.
66. Gao B-C, Montes MJ, Davis CO, Goetz AF. Atmospheric correction algorithms for hyperspectral remote sensing data of land and ocean. Remote sensing of environment. 2009;113:S17-S24.
67. Moses WJ, Gitelson AA, Perk RL, Gurlin D, Rundquist DC, Leavitt BC, et al. Estimation of chlorophyll-a concentration in turbid productive waters using airborne hyperspectral data. Water research. 2012;46(4):993-1004.
68. Scaramuzza P, Barsi J, editors. Landsat 7 scan line corrector-off gap-filled product development. Proceeding of Pecora; 2005.
69. Asraf HM, Nooritawati M, Rizam MS. A comparative study in kernel-based support vector machine of oil palm leaves nutrient disease. Procedia Engineering. 2012;41:1353-9.

70. Research Systems Inc. ENVI Tutorial. 5.3.1 ed2015. p. ENVI Software Package.
71. Fahad S, Su F, Wei K. Quantifying households' vulnerability, regional environmental indicators, and climate change mitigation by using a combination of vulnerability frameworks. Land Degradation & Development. 2023;34(3):859-72.
72. Tauqeer HM, Turan V, Farhad M, Iqbal M. Sustainable agriculture and plant production by virtue of biochar in the era of climate change. Managing plant production under changing environment: Springer; 2022. p. 21-42.
73. Fathi-Taperasht A, Shafizadeh-Moghadam H, Kouchakzadeh M. MODIS-based evaluation of agricultural drought, water use efficiency and post-drought in Iran; considering the influence of heterogeneous climatic regions. Journal of Cleaner Production. 2022;374:133836.
74. Modarres R, Sarhadi A, Burn DH. Changes of extreme drought and flood events in Iran. Global and Planetary Change. 2016;144:67-81.
75. Mehravar S, Amani M, Moghimi A, Javan FD, Samadzadegan F, Ghorbanian A, et al. Temperature-Vegetation-soil Moisture-Precipitation Drought Index (TVMPDI); 21-year drought monitoring in Iran using satellite imagery within google Earth engine. Advances in space research. 2021;68(11):4573-93.
76. General Department of Meteorology of Kerman province; [Available from: www.kerman-met.ir.]